Electrocatalysis

International Edition: DOI: 10.1002/anie.201811667
German Edition: DOI: 10.1002/ange.201811667

Lateral Adsorbate Interactions Inhibit $HCOO^-$ while Promoting CO Selectivity for CO_2 Electrocatalysis on Silver

*Divya Bohra, Isis Ledezma-Yanez, Guanna Li, Wiebren de Jong, Evgeny A. Pidko, and Wilson A. Smith**

Abstract: *Ag is a promising catalyst for the production of carbon monoxide (CO) via the electrochemical reduction of carbon dioxide (CO_2ER). Herein, we study the role of the formate ($HCOO^-$) intermediate *OCHO, aiming to resolve the discrepancy between the theoretical understanding and experimental performance of Ag. We show that the first coupled proton-electron transfer (CPET) step in the CO pathway competes with the Volmer step for formation of *H, whereas this Volmer step is a prerequisite for the formation of *OCHO. We show that *OCHO should form readily on the Ag surface owing to solvation and favorable binding strength. In situ surface-enhanced Raman spectroscopy (SERS) experiments give preliminary evidence of the presence of O-bound bidentate species on polycrystalline Ag during CO_2ER which we attribute to *OCHO. Lateral adsorbate interactions in the presence of *OCHO have a significant influence on the surface coverage of *H, resulting in the inhibition of $HCOO^-$ and H_2 production and a higher selectivity towards CO.*

The electrochemical reduction of CO_2 is a very promising approach providing a means to manage intermittent renewable electricity production by converting it into a chemically valuable form, while recycling climate change-inducing CO_2.[1] Understanding the pathways for the (electro)chemical transformations involved in CO_2ER is critical to advance its technological utilization. The two-proton-electron transfer products of CO_2ER, namely CO and $HCOO^-$ are highly attractive owing to the relatively low overpotentials needed to drive their production, and high achievable Faradaic efficiencies.[2,3] The need to balance the performance with low cost electrodes has led to an increased interest in using Ag as a CO_2 reduction catalyst, which has a high selectivity to CO while being 100-times cheaper than the alternative Au.[2,4,5]

It is widely accepted that the formation of CO from CO_2 on transition metal catalysts with an aqueous electrolyte proceeds via the *COOH species, whereas the formation of $HCOO^-$ proceeds via the bidentate O-bound *OCHO species, both forming after a single CPET step.[4,6–10] Consideration of the relative limiting potentials (U_L) alone dictates that the formation of H_2 is most thermodynamically feasible on Ag(110), followed by $HCOO^-$ and then CO (see Figure S2 in the Supporting Information; Figure S1 depicts the limiting potentials with varying surface facets of Ag). Interestingly, this conclusion does not reconcile with the experimental observations of the formation of CO as the major product of CO_2ER on Ag, H_2 as a by-product (through the hydrogen evolution reaction, HER), with the detection of only trace amounts of $HCOO^-$ for intermediate applied potentials of ca. −0.9 V to −1.3 V.[4] For applied potentials more or less negative of this range, the Faradaic efficiency for H_2 dominates that for CO. However, irrespective of the applied potential, the experimentally observed Faradaic efficiency for the formation of $HCOO^-$ remains significantly lower (<10%) relative to CO and H_2. The reasons for this discrepancy and the role of the stable species *OCHO in the catalytic performance of Ag is not well understood.

Herein we report our findings of the mechanistic differences in the formation of *OCHO and *COOH and their respective interactions with the H_2 production pathways on an Ag(110) surface. We show that there are two major bifurcations in the reaction mechanism before and after formation of *H that control the selectivity between CO, $HCOO^-$ and H_2. We present reaction barrier calculations to show that the formation of *OCHO has a significantly lower kinetic barrier relative to *COOH on Ag(110) and that solvation of the transition state by the surrounding water molecules plays an important role in determining this barrier. Finally, we demonstrate that the influence of lateral adsorbate-adsorbate interactions resulting from the presence of *OCHO on the surface promotes CO production while inhibiting itself and the formation of $HCOO^-$ as a consequence.

The lowest unoccupied molecular orbital (LUMO) of a bent CO_2 is highly localized at the C, whereas the highest occupied molecular orbital (HOMO) is highly localized at the O, making them strongly susceptible to interactions with

[*] D. Bohra, W. A. Smith
Materials for Energy Conversion and Storage (MECS)
Department of Chemical Engineering
Delft University of Technology
2629 HZ Delft (The Netherlands)
E-mail: W.Smith@tudelft.nl
I. Ledezma-Yanez, W. de Jong
Large-Scale Energy Storage (LSE), Department of Process and Energy, Delft University of Technology
2629 HZ Delft (The Netherlands)
G. Li, E. A. Pidko
Inorganic Systems Engineering (ISE), Department of Chemical Engineering, Delft University of Technology
2629 HZ Delft (The Netherlands)

Supporting information (Computational and experimental details along with auxiliary computational results and in situ SERS results) and the ORCID identification number(s) for the author(s) of this article can be found under: https://doi.org/10.1002/anie.201811667.

nucleophiles and electrophiles, respectively.[6] We use Bader charge analysis[11] to quantify this susceptibility and to chart the reaction path for the first CPET step for CO_2 reduction, as depicted in Figure 1. For the C–H bond of *OCHO to form, *H with a partial negative charge (δ^-) acts as a nucleophile for the $C^{\delta+}$ of CO_2 (top panel in Figure 1). Both Volmer–Tafel

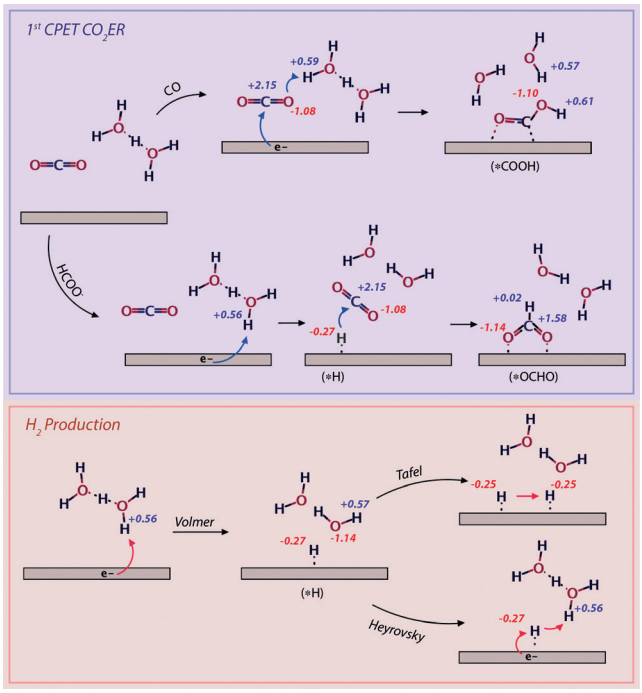

Figure 1. Schematic representation of the first reduction step for CO_2ER pathways to form *COOH (CO pathway) and *OCHO ($HCOO^-$ pathway) on an Ag(110) surface (violet box above) along with the two H_2 formation pathways: Volmer–Tafel and Volmer–Heyrovsky (peach box below). The excess partial charges for the relevant chemical species are in blue for a excess positive charge and in red for excess negative charge.

and Volmer–Heyrovsky mechanisms for the formation of H_2 also share the first CPET Volmer step of $*H^{\delta-}$ formation (bottom panel in Figure 1). This implies that the formation of *COOH competes with the Volmer step which is in-turn a prerequisite for the formation of *OCHO. Following the Volmer step, the *H can either participate in a Tafel or Heyrovsky step to form H_2, or react with the CO_2 to form *OCHO. According to our analysis, there are therefore two reaction bifurcations before and after formation of *H that generally control the selectivity for CO_2ER. An analogous finding has been recently reported for CO_2ER on Cu(100) surfaces[12] and as well as for the selectivity of CO_2ER on metalloporphyrins.[13]

This approach can be further extended to the formation of higher CPET products from CO_2ER such as methanol (CH_3OH) and methane (CH_4; see extended reaction scheme in Figure S8). The thermodynamically most feasible routes for the formation of CH_3OH and CH_4 go via *COOH followed by the *CHO species, as becomes clear from the U_L for the various reaction pathways shown in Figures S9 and S10. Extending the Bader charge analysis to these pathways, it is expected that the formation of *CHO from *CO forms through a surface bound *H interacting with the $C^{\delta+}$. Θ_{*H} is therefore expected to play an important role in the formation of higher electron reduction products of CO_2ER and this analysis can potentially be useful for studying catalysts such as Cu where these reaction steps become prominent. Interestingly, very recent experimental findings for CO_2ER on Cu catalysts draw similar conclusions and indicate an important role of *H in the formation of CH_4.[14]

Climbing image nudged elastic band (CI-NEB) calculations were performed to estimate the height of the activation barriers based on the reaction path analysis presented in Figure 1 (see Computational Details section in Supporting Information). As can be seen in Figure 2, the activation

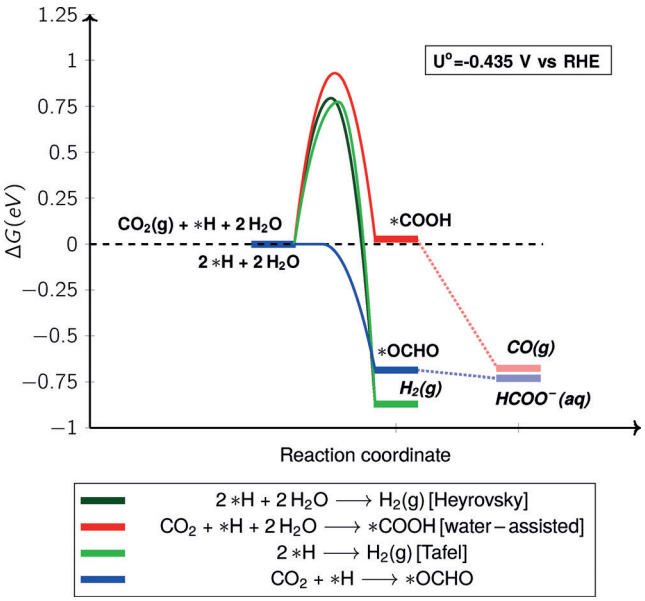

Figure 2. Free energy of activation corrected for solvation for Ag(110) at a reference potential $U^\circ = -0.435$ V vs. RHE for the equilibrium between surface bound *H and the bulk proton and electron pair.

barriers after correction for solvation for formation of *COOH is 0.93 eV and for H_2 generation following Heyrovsky and Tafel mechanisms are 0.79 eV, and 0.77 eV, respectively, with H_2 as the most thermodynamically favorable product. Interestingly however, there is no kinetic barrier for the formation of *OCHO involving the direct nucleophilic attack by *H (see Figures S3–S6 for uncorrected activation barriers, atomic configurations and excess partial charges of the initial, transition and final states). The high solvation energy of the transition state relative to the initial state for *OCHO (Table S1, Figure S7) plays an important role in diminishing the activation barrier for its formation. This analysis highlights the importance of the consideration of solvation in theoretical mechanistic studies for CO_2ER; a conclusion which is in agreement with what has been shown for other (electro)catalytic systems.[15] The presence of cationic and anionic species in the electrolyte may also influence the binding energies and activation barriers for the formation of certain reaction intermediates and there are

ongoing efforts to include these effects in computational studies pertaining to CO_2ER.[16] Based on the results in Figure 2, we show that there is a significant energy barrier for the formation of the CO pathway intermediate *COOH, whereas *OCHO is expected to form readily on the Ag(110) surface in the presence of *H.

To validate our theoretical findings, preliminary in situ electrochemical SERS measurements were performed to probe polycrystalline Ag catalyst surface during CO_2ER in 0.05 M $Li_2B_4O_7$[17] saturated with CO_2, with a bulk pH of 6.1 (Experimental details in Supporting Information). We observe a double-band shape at 1436 and 1469 cm^{-1} (Figure 3) corresponding to an O-bound bidentate intermediate on the Ag surface, which we believe to be the *OCHO species based on similar evidence obtained in literature for carboxylate species on silver hydrosols.[18] The interactions of O-bound species with the Ag surface appear at relatively low overpotentials (−0.52 V vs. RHE), in agreement with the obtained theoretical results. We also observe a correlation in the appearance of a δC–H vibration band at 1298 cm^{-1} [19] with the bidentate signal merging into a broader band at more cathodic potentials of −1.12 V vs. RHE as can be seen in Figure 3. The same correlation is observed using a lithium borate buffer solution with a bulk pH of 6.9 albeit at higher overpotentials (Figure S25). These experiments suggest that pH plays an important role in CO_2ER at lower overpotentials due to its implications on the formation of *H on the Ag electrode.

Adsorbate–adsorbate interactions play an important role in determining the energetics of surface reactions including CO_2ER.[20,21] Considering the high likelihood of the presence of *OCHO species on the Ag catalyst surface, we investigate its influence on the adsorption energies of reaction intermediates involved in the two-electron reduction processes during CO_2ER. The free energy diagram for Ag(110) in Figure 4 shows that the presence of *OCHO weakens the *H binding significantly (green pathway in Figure 4 and Figure S12) whereas the effect of its presence on the binding energies of the *COOH, *OCHO, and *CO species is relatively smaller. As a result, the U_L for the formation of H_2 and $HCOO^-$ (both proceeding via the Volmer step), become much less favorable and comparable to the U_L for the formation of CO.

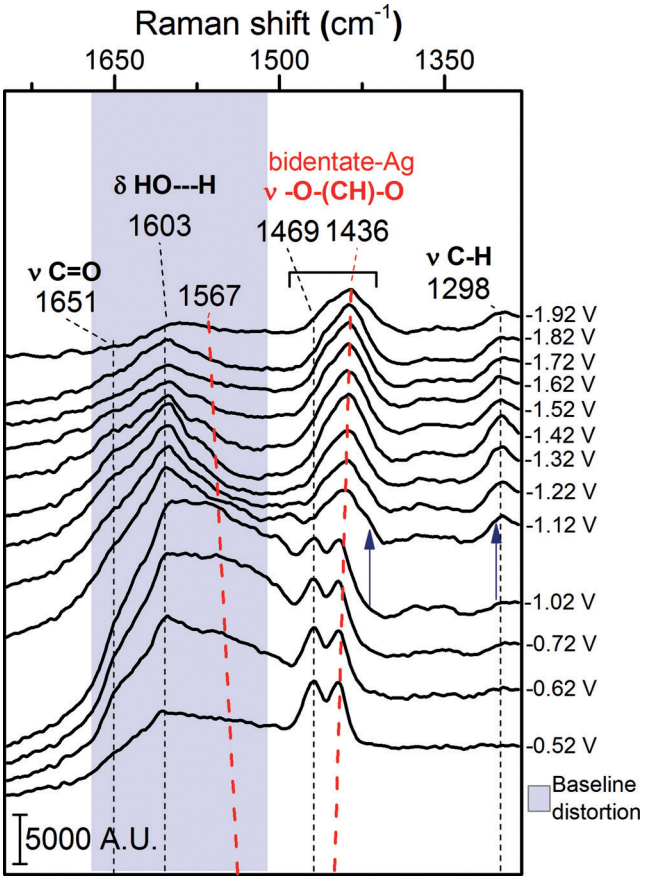

Figure 3. SERS spectra for CO_2ER on polycrystalline Ag in 0.05 M $Li_2B_4O_7$ saturated with CO_2 with a bulk pH of 6.1. The spectral region shows the O-bound bidentate species and the shift towards lower frequencies as we apply more cathodic potentials. The blue arrows indicate the formation of a new band at 1298 cm^{-1} related to the merging and shift of the bidentate bands. All potentials are given vs. RHE.

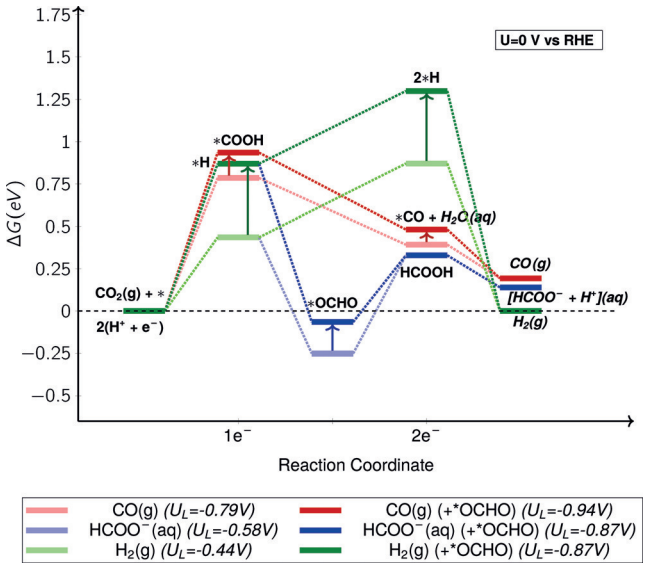

Figure 4. Free-energy diagram for formation of CO(g), $HCOO^-$(aq) and H_2(g) on Ag(110) surface at 0 V vs. RHE. The adsorption energies shown in dark red, blue and green are in the presence of *OCHO ($\Theta = 1/3$), whereas the energies in light red, blue, and green are without *OCHO. The upward arrows denote the change in free energy of the respective intermediates because of the presence of *OCHO on the surface. Formation of *OCHO has been shown to occur following the formation of *H as per the proposed mechanism and is not an electron-transfer step. Limiting potentials (U_L) are given vs. RHE. The free energy values have been corrected for solvation (see Table S1).

Figure S11 shows the effect of the coverage of *H (Θ_{*H}) on the binding energy of *COOH for Ag(110). It is clear that as Θ_{*H} increases, the binding of *COOH on the catalyst surface becomes increasingly thermodynamically unfavorable. The presence of *OCHO therefore has two important consequences for the selectivity of Ag CO_2ER catalysts: firstly, *OCHO weakens the binding strength of *H with the

catalyst surface, bringing the CO formation pathway to a level-playing field thermodynamically with the H_2 and $HCOO^-$ pathways. Secondly, the lower Θ_{*H} as a consequence of the weaker *H binding enables the formation of *COOH, thereby improving the selectivity of the catalyst towards CO. The influence of lateral adsorbate interaction of *OCHO on the binding strength of *H diminishes as the activity of the catalytic surface reduces (see Figure S13). The lower binding strength of *COOH in addition to the negligible effect on the binding strength of *H in the presence of *OCHO for Ag(111) (Figure S14) is in line with the experimental observation that close-packed surfaces such as Ag(111) have drastically lower activity for CO_2ER to CO relative to Ag(110).[22] This analysis highlights the importance of the consideration of lateral adsorbate–adsorbate interactions to bridge the discrepancy between theoretical predictions and the experimental observations for Ag as well as other CO_2ER catalysts.

From our theoretical analysis, we come to the conclusion that the O-bound formate precursor species *OCHO, which is typically considered irrelevant for the CO producing catalyst Ag, should not only be present on the surface at low overpotentials during CO_2ER, but is also likely playing an active role in promoting the selectivity of Ag towards CO production. In addition, the results strongly indicate that factors such as Θ_{*H} and solvation by surrounding water molecules will play an important role in controlling selectivity between the various CO_2ER products. Calculation of activation barriers at constant potential and adjusted for activities of reactant and electrolyte species in order to simulate the conditions during electrocatalysis remains a challenge and there is a need for further development of computational methodologies for this purpose. Our approach demonstrates a constructive interplay between theory and experiments to advance the understanding of a complex system of high practical significance. The results highlight the need to study the catalyst surface in its operational steady state, both theoretically and experimentally, to understand the cooperative and competitive effects between the reaction species that ultimately result in the observed performance.

Acknowledgements

The authors thank NWO for support via the VIDI grant (WAS and DB). G.L. acknowledges the financial support from NWO for the personal VENI grant (no. 016.Veni.172.034).

Conflict of interest

The authors declare no conflict of interest.

Keywords: adsorbate-adsorbate interactions · in situ studies · DFT · electrocatalysis · Raman spectroscopy

How to cite: *Angew. Chem. Int. Ed.* **2019**, *58*, 1345 – 1349
Angew. Chem. **2019**, *131*, 1359 – 1363

[1] a) Q. Lu, F. Jiao, *Nano Energy* **2016**, *29*, 439 – 456; b) D. T. Whipple, P. J. A. Kenis, *J. Phys. Chem. Lett.* **2010**, *1*, 3451 – 3458; c) M. Gattrell, N. Gupta, A. Co, *Energy Convers. Manage.* **2007**, *48*, 1255 – 1265; d) O. Edenhofer et al., *IPCC, 2014: Climate Change 2014: Mitigation of Climate Change. Contribution of Working Group III, to the Fifth Assessment Report of the Intergovernmental Panel on Climate Change*, **2014**; e) D. A. Tryk, A. Fujishima, *Electrochem. Soc. Interface* **2001**, 32 – 36.

[2] S. Verma, B. Kim, H.-R. Jhong, S. Ma, P. J. A. Kenis, *ChemSusChem* **2016**, *9*, 1972 – 1979.

[3] a) M. T. Koper, *J. Electroanal. Chem.* **2011**, *660*, 254 – 260; b) J. Durst, A. Rudnev, A. Dutta, Y. Fu, J. Herranz, V. Kaliginedi, A. Kuzume, A. A. Permyakova, Y. Paratcha, P. Broekmann, T. J. Schmidt, *Chimia* **2015**, *69*, 769 – 776; c) G. Centi, S. Perathoner, *Catal. Today* **2009**, *148*, 191 – 205; d) C. Oloman, H. Li, *ChemSusChem* **2008**, *1*, 385 – 391; e) C. Song, *Catal. Today* **2006**, *115*, 2 – 32.

[4] T. Hatsukade, K. P. Kuhl, E. R. Cave, D. N. Abram, T. F. Jaramillo, *Phys. Chem. Chem. Phys.* **2014**, *16*, 13814 – 13819.

[5] a) M. Ma, B. J. Trześniewski, J. Xie, W. A. Smith, *Angew. Chem. Int. Ed.* **2016**, *55*, 9748 – 9752; *Angew. Chem.* **2016**, *128*, 9900 – 9904; b) A. Seifitokaldani, C. M. Gabardo, T. Burdyny, C.-T. Dinh, J. P. Edwards, M. G. Kibria, O. S. Bushuyev, S. O. Kelley, D. Sinton, E. H. Sargent, *J. Am. Chem. Soc.* **2018**, *140*, 3833 – 3837; c) Y. Yoon, A. S. Hall, Y. Surendranath, *Angew. Chem. Int. Ed.* **2016**, *55*, 15282 – 15286; *Angew. Chem.* **2016**, *128*, 15508 – 15512; d) Q. Lu, J. Rosen, F. Jiao, *ChemCatChem* **2015**, *7*, 38 – 47; e) C. Kim, H. S. Jeon, T. Eom, M. S. Jee, H. Kim, C. M. Friend, B. K. Min, Y. J. Hwang, *J. Am. Chem. Soc.* **2015**, *137*, 13844 – 13850; f) J. Rosen, G. S. Hutchings, Q. Lu, S. Rivera, Y. Zhou, D. G. Vlachos, F. Jiao, *ACS Catal.* **2015**, *5*, 4293 – 4299.

[6] A. M. Appel, et al., *Chem. Rev.* **2013**, *113*, 6621 – 6658.

[7] R. Kortlever, J. Shen, K. J. P. Schouten, F. Calle-Vallejo, M. T. M. Koper, *J. Phys. Chem. Lett.* **2015**, *6*, 4073 – 4082.

[8] J. S. Yoo, R. Christensen, T. Vegge, J. K. Nørskov, F. Studt, *ChemSusChem* **2016**, *9*, 358 – 363.

[9] J. T. Feaster, C. Shi, E. R. Cave, T. Hatsukade, D. N. Abram, K. P. Kuhl, C. Hahn, J. K. Nørskov, T. F. Jaramillo, *ACS Catal.* **2017**, *7*, 4822 – 4827.

[10] A. Bagger, W. Ju, A. S. Varela, P. Strasser, J. Rossmeisl, *ChemPhysChem* **2017**, *18*, 3266 – 3273.

[11] a) R. F. W. Bader, *Atoms in Molecules: A Quantum Theory*, Oxford University Press, New York, **1994**; b) W. Tang, E. Sanville, G. Henkelman, *J. Phys. Condens. Matter* **2009**, *21*, 084204.

[12] T. Cheng, H. Xiao, W. A. Goddard, *J. Am. Chem. Soc.* **2016**, *138*, 13802 – 13805.

[13] A. J. Göttle, M. T. M. Koper, *J. Am. Chem. Soc.* **2018**, *140*, 4826 – 4834.

[14] a) M. Schreier, Y. Yoon, M. N. Jackson, Y. Surendranath, *Angew. Chem. Int. Ed.* **2018**, *57*, 10221 – 10225; *Angew. Chem.* **2018**, *130*, 10378 – 10382; b) X. Nie, M. R. Esopi, M. J. Janik, A. Asthagiri, *Angew. Chem. Int. Ed.* **2013**, *52*, 2459 – 2462; *Angew. Chem.* **2013**, *125*, 2519 – 2522.

[15] a) C. Michel, J. Zaffran, A. M. Ruppert, J. Matras-Michalska, M. Jędrzejczyk, J. Grams, P. Sautet, *Chem. Commun.* **2014**, *50*, 12450 – 12453; b) D. Loffreda, C. Michel, F. Delbecq, P. Sautet, *J. Catal.* **2013**, *308*, 374 – 385; c) Y. Sha, T. H. Yu, Y. Liu, B. V. Merinov, W. A. Goddard, *J. Phys. Chem. Lett.* **2010**, *1*, 856 – 861.

[16] a) L. D. Chen, M. Urushihara, K. Chan, J. K. Nørskov, *ACS Catal.* **2016**, *6*, 7133 – 7139; b) J. Resasco, L. D. Chen, E. Clark, C. Tsai, C. Hahn, T. F. Jaramillo, K. Chan, A. T. Bell, *J. Am. Chem. Soc.* **2017**, *139*, 11277 – 11287.

[17] a) I. Ledezma-Yanez, W. D. Z. Wallace, P. Sebastián-Pascual, V. Climent, J. M. Feliu, M. T. M. Koper, *Nat. Energy* **2017**, *2*, 17031;

b) J. Rossmeisl, K. Chan, R. Ahmed, V. Tripković, M. E. Björketun, *Phys. Chem. Chem. Phys.* **2013**, *15*, 10321 – 10325.
[18] S. Kai, W. Chaozhi, X. Guangzhi, *Spectrochim. Acta Part A* **1989**, *45*, 1029 – 1032.
[19] H. Edwards, J. M. Chalmers in *Handbook of Vibrational Spectroscopy* (Eds.: J. M. Chalmers, P. R. Griffiths), Wiley, New York, **2006**, pp. 1887 – 1890.
[20] L. C. Grabow, B. Hvolbæk, J. K. Nørskov, *Top. Catal.* **2010**, *53*, 298 – 310.
[21] E. R. Cave, C. Shi, K. P. Kuhl, T. Hatsukade, D. N. Abram, C. Hahn, K. Chan, T. F. Jaramillo, *ACS Catal.* **2018**, *8*, 3035 – 3040.
[22] N. Hoshi, M. Kato, Y. Hori, *J. Electroanal. Chem.* **1997**, *440*, 283 – 286.

Manuscript received: October 10, 2018
Accepted manuscript online: November 16, 2018
Version of record online: December 18, 2018

